EFFECT OF BEAM CHROMATICITY ON FOREGROUNDS IN WIDE-FIELD MEASUREMENTS OF REDSHIFTED 21 CM POWER SPECTRA

Nithyanandan Thyagarajan[1][*], TBD
Draft version January 28, 2016

ABSTRACT

Keywords: cosmology: observations — dark ages, reionization, first stars — large-scale structure of universe — methods: statistical — radio continuum: galaxies — techniques: interferometric

1. INTRODUCTION

The period in the history of the Universe characterized by the transition of neutral hydrogen in the intergalactic medium (IGM) to a fully ionized state due to the formation of radiating objects such as the first stars and galaxies is referred to as the Epoch of Reionization (EoR). This is an important period of nonlinear growth of matter density perturbations and astrophysical evolution leading to the large scale structure observed currently in the Universe. And yet, this period in the Universe's history has remained poorly probed to date with observations.

The redshifted neutral hydrogen from the IGM in this epoch has been identified to be one of the most promising and direct probes of the EoR (Sunyaev & Zeldovich 1972; Scott & Rees 1990; Madau et al. 1997; Tozzi et al. 2000; Iliev et al. 2002). Numerous experiments using low frequency radio telescopes targeting the redshifted 21 cm line from the spin-flip transition of HI have become operational such as the Murchison Widefield Array (MWA; Lonsdale et al. 2009; Bowman et al. 2013; Tingay et al. 2013), the Precision Array for Probing the Epoch of Reionization (PAPER; Parsons et al. 2010), the Low Frequency Array (LOFAR; van Haarlem et al. 2013) and the Giant Metrewave Radio Telescope EoR experiment (GMRT; Paciga et al. 2013). These instruments have sufficient sensitivity for a statistical detection of the EoR signal via estimating the spatial power spectrum of the redshifted HI temperature fluctuations (Beardsley et al. 2013; Thyagarajan et al. 2013). These instruments are intended to be precursors and pathfinders to the next generation of low frequency radio observatories such as the Hydrogen Epoch of Reionization Array[3] (HERA; DeBoer et al. 2015) and the Square Kilometre Array[4] (SKA). These next-generation instruments will advance the capability from a mere statistical detection of the signal to a direct three-dimensional tomographic imaging of the HI during the EoR.

The most significant challenge to low frequency EoR observations arises from the extremely bright Galactic and extragalactic foreground synchrotron emission which are $\sim 10^4$ times stronger than the desired EoR signal (Di Matteo et al. 2002; Ali et al. 2008; Bernardi et al. 2009, 2010; Ghosh et al. 2012). All the current and future instruments rely on the inherent differences in spatial isotropy and spectral smoothness between the EoR signal and the foregrounds to extract the EoR power spectrum (see, e.g., Furlanetto & Briggs 2004; Morales & Hewitt 2004; Zaldarriaga et al. 2004; Santos et al. 2005; Furlanetto et al. 2006; McQuinn et al. 2006; Morales et al. 2006; Wang et al. 2006; Gleser et al. 2008).

When expressed in the coordinate system of power spectrum measurements described by the three-dimensional wavenumber (k), the foreground emission is restricted to a wedge-shaped region commonly referred to as the *foreground wedge* (Bowman et al. 2009; Liu et al. 2009, 2014a,b; Datta et al. 2010; Liu & Tegmark 2011; Ghosh et al. 2012; Morales et al. 2012; Parsons et al. 2012; Trott et al. 2012; Vedantham et al. 2012; Dillon et al. 2013; Pober et al. 2013; Thyagarajan et al. 2013; Dillon et al. 2014) whereas the EoR signal has spherical symmetry due to its isotropy which appears elongated along line of sight k modes due to peculiar velocity effects when dominated by matter density perturbations during early stages of reionization. The extreme dynamic range required to subtract foregrounds precisely demands high precision modeling of foregrounds as observed by modern wide-field instruments (Thyagarajan et al. 2015b,a).

2. THE HYDROGEN EPOCH OF REIONIZATION ARRAY

DeBoer et al.(2016)

3. DELAY SPECTRUM

(Parsons et al. 2012)

3.1. *The Wide-Field "Pitchfork" Effect*

(Thyagarajan et al. 2015b,a)

4. SIMULATIONS

We simulate wide-field visibilities for 19-element HERA from all-sky antenna power pattern and foreground models using the PRISim[5] software package. The simulations cover 24 hr of observation in *drift* mode consisting of 80 accumulations spanning 1080 s each. The total bandwidth is 100 MHz centered on 150 MHz consisting of 128 channels with 781.125 kHz frequency resolution each. Models of the antenna power pattern and foregrounds are described below.

4.1. *Antenna Power Pattern*

(Neben et al. 2015)

---

[1] Arizona State University, School of Earth and Space Exploration, Tempe, AZ 85287, USA
[*] e-mail: t_nithyanandan@asu.edu
[3] http://reionization.org/
[4] https://www.skatelescope.org/

[5] The Precision Radio Interferometry Simulator (PRISim) is publicly available at https://github.com/nithyanandan/PRISim

4.2. *Foreground Model*

Our all-sky foreground model is the same as the one in Thyagarajan et al. (2015b). It consists of diffuse emission (de Oliveira-Costa et al. 2008) and point sources. The latter is obtained from a combination of the NRAO VLA Sky Survey (NVSS; Condon et al. 1998) at 1.4 GHz and the Sydney University Molonglo Sky Survey (SUMSS; Bock et al. 1999; Mauch et al. 2003) at 843 MHz with a mean spectral index of -0.83. The diffuse sky model has an angular resolution of $13'.74$.

5. CHROMATICITY OF POWER PATTERN

The equation for delay spectrum describes the mapping between sky location of a foreground object and delay. The chromatic nature (variation with frequency) of the antenna power pattern results in a convolution of the geometrical mapping with the delay response of spectral chromaticity of the power pattern. This can result in a significant spillover of foreground power beyond the horizon delay limits especially in the case of foregrounds near the horizon.

Fig. 1 demonstrates the beyond-the-horizon spillover even from a flat-spectrum point source at different off-axis angles. The three panels correspond to delay spectra from different positions of the point source – $0°$(left), $45°$(middle) and $89°$(right) – from the zenith. The phase centers are located at the source positions and hence the delay spectra are centered on $\tau = 0$ ns. The response of the simulated dish power pattern (dashed line) is comapred with that from an *Airy* pattern resulting from a nominal uniformly illuminated circular disk (solid line). The gray vertical lines correspond to the horizon limits at ±48.7 ns for a 14.6 m antenna spacing. In all these cases, a *Blackman-Harris* window function has been applied along the spectral axis.

At $0°$off-axis, the *Airy* pattern has no spectral variation except that introduced by the *Blackman-Harris* window function and thus reproduces its Fourier response centered at $\tau = 0$ ns whereas the simulated power pattern is found to exhibit some spectral variation giving rise to the wings on either side of $\tau = 0$ ns. As off-axis angle increases to $45°$, both the power patterns clearly exhibit chromaticity. The simulated pattern not only has a higher magnitude inside the horizon limits (by a factor ~ 10) but also exhibits higher chromaticity (by many orders of magnitude) in modes beyond the horizon relative to that of an *Airy* pattern. In contrast, at $89°$off-axis, not only does the simulated pattern have higher chromaticity in high delay modes but is also two orders of magnitude higher in amplitude inside the horizon limits relative to the nominal *Airy* pattern.

It is important to note that in a generic scenario where visibilities are not phased to a specific foreground location, the chromaticity of the power pattern will imprint itself on location of the foreground objects in delay space and will give rise to significant spillover especially from foregrounds near the horizon.

We investigate the effects of spectral chromaticity of the power pattern in more detail below.

5.1. *Directional Chromaticity of Power Pattern*

We generalize the analysis above by computing the delay power spectrum of the power pattern along its spectral axis in every direction in an effort to study its performance as a function of angle on the sky.

$$A'(l, m, \tau) = \int A(l, m, f) \, e^{-j2\pi f\tau} \, \mathrm{d}f \qquad (1)$$

We define the directional chromaticity of antenna power pattern as:

$$C(l, m) = \frac{\int\limits_{|\tau|>60\,\mathrm{ns}} |A'|^2 \, \mathrm{d}\tau}{\int\limits_{|\tau|>60\,\mathrm{ns}} \mathrm{d}\tau} \qquad (2)$$

where, the limit $|\tau| > 60$ ns was chosen to represent a region well beyond the horizon limits (±48.7 ns) for a 14.6 m antenna spacing. It thus measures the average power arising out of chromaticity in each delay mode beyond $|\tau| > 60$ ns.

Fig. 2 shows the directional chromaticity, $C(l, m)$, of the power patterns of an *Airy* disk for reference (left) and a simulated disk (middle) on an orthographic projection onto direction cosines. Their color scale is shown at the top for reference. The chromaticity of the *Airy* pattern is symmetric and always below 500. On the other hand, a simulated disk exhibits higher levels of chromaticity in the range 100–50,000. The ratio of their chromaticities is shown on the right with corresponding color scale on its right. The simulated disk is more chromatic than the nominal *Airy* disk by a factor between 100 and up to 10000. However, chromaticity in regions near the horizon which map to the horizon limits in the delay spectrum and have the most significant impact on spillover into the *EoR window* in the simulated disk are higher than that of an *Airy* disk only by factors $\lesssim 4$. Thus the simulated disk for HERA achieves reasonable control on the chromaticity near the horizon despite the very high levels near the center.

Also shown are the tracks (black dots) of point sources brighter than 50 Jy in the LST range 0–12 hrs. The solid circle near the bottom denotes the south celestial pole. It is noted that there are a few bright point sources that spend a majority of time in this LST range near the northern and southern horizons which will contaminate the measured visibilities on north-south antenna spacings. Future simulations of the dish power pattern must take the bright foreground locations, especially near the horizon, into account.

### 5.2. *Effect on Delay Power Spectrum*

Now we consider the effect of chromaticity of the power pattern on the delay power spectrum.

We simulate visibilities from our foreground model using three different models for the antenna power pattern – *Airy* pattern, simulated dish, and a pattern at 150 MHz of the simulated dish assumed to be achromatic over the entire band.

Fig. 3 shows the delay power spectra of foregrounds obtained with the aforementioned models for power pattern. In all these panels, power spectra obtained with achromatic, *Airy* disk and simulated disk are shown in black, red, and blue respectively. The vertical gray lines denote the horizon limits for a 14.6 m antenna spacing. The full band delay power spectra of the foregrounds measured on a 14.6 m antenna spacing ori-
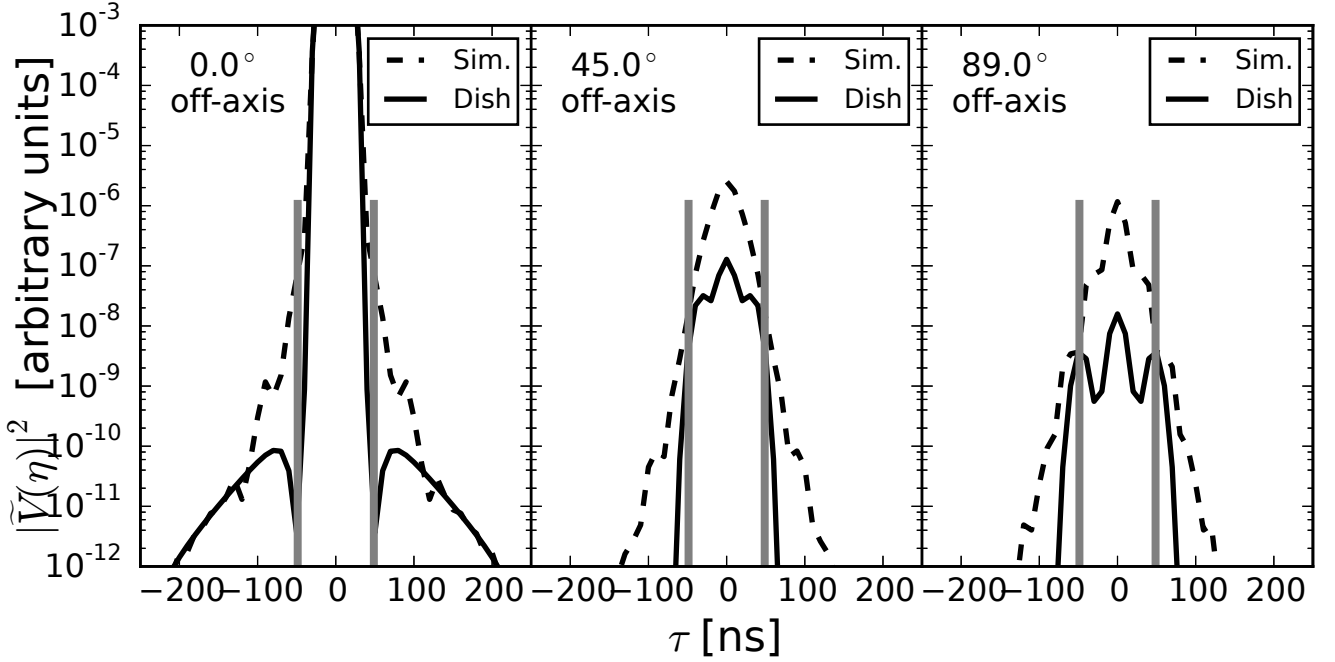
Figure 1. Chromaticity of antenna power pattern at directions off-axis.
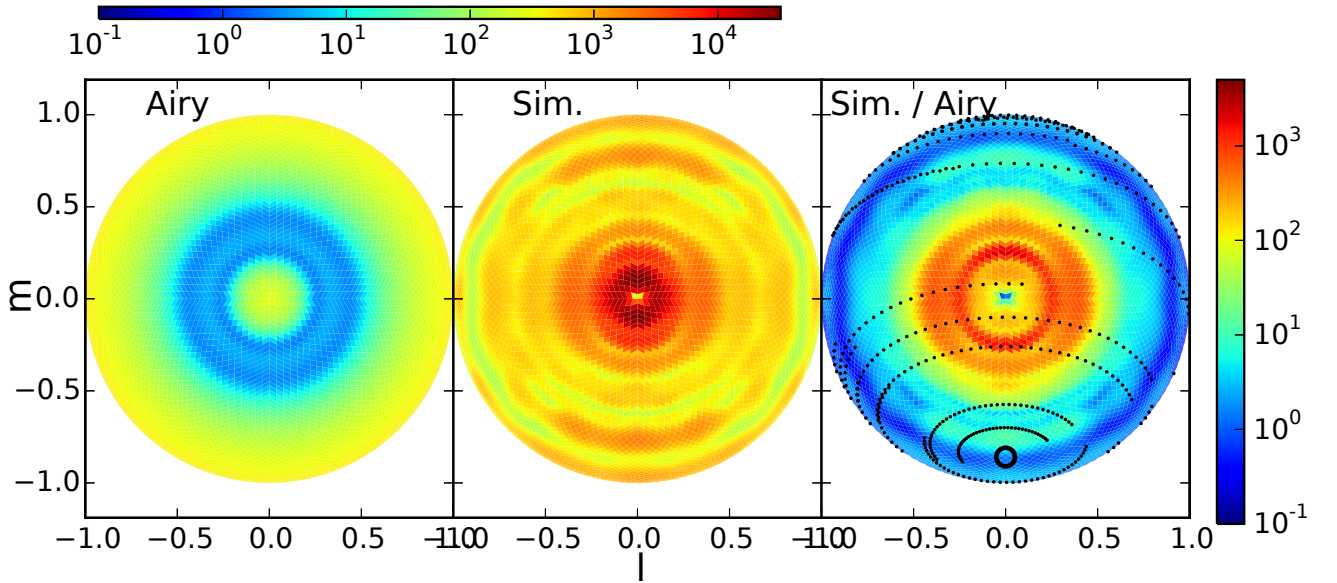

Figure 2. All-sky directional chromaticity of antenna power pattern.

ented eastward is shown in the top left panel. A clear trend of broadening of spillover-wings outside the horizon limits is seen with increasing chromaticity. For instance, the spillover from foreground delay power spectrum obtained with simulated dish pattern extends out to $k_\parallel \approx \pm 0.14\,h\,\mathrm{Mpc}^{-1}$, with the *Airy* pattern it extends out to $k_\parallel \approx \pm 0.08\,h\,\mathrm{Mpc}^{-1}$, while the achromatic beam extends it only out to $k_\parallel \approx \pm 0.05\,h\,\mathrm{Mpc}^{-1}$. Thus an increase in chromaticity extends the foreground spillover into higher $k_\parallel$-modes making them inaccessible for EoR H I signal detection.

Following the foreground removal strategy, the top middle panel shows these foreground delay spectra de-convolved using the complex delay CLEAN algorithm (Taylor et al. 1999; Parsons & Backer 2009; Parsons et al. 2012). The CLEAN window covers delay bins between the horizon delay limits and extends further by three delays bins on each side of the horizon limit where a delay bin is of size inverse of the bandwidth. The panel at the top right shows the residuals left behind after deconvolution.

Owing to the chromaticity of power patterns, the spillover from foregrounds extends beyond the horizon limits, most severely in the simulated disk pattern. As a result the residuals have significant power remaining on either side of the horizon limits since the window for de-
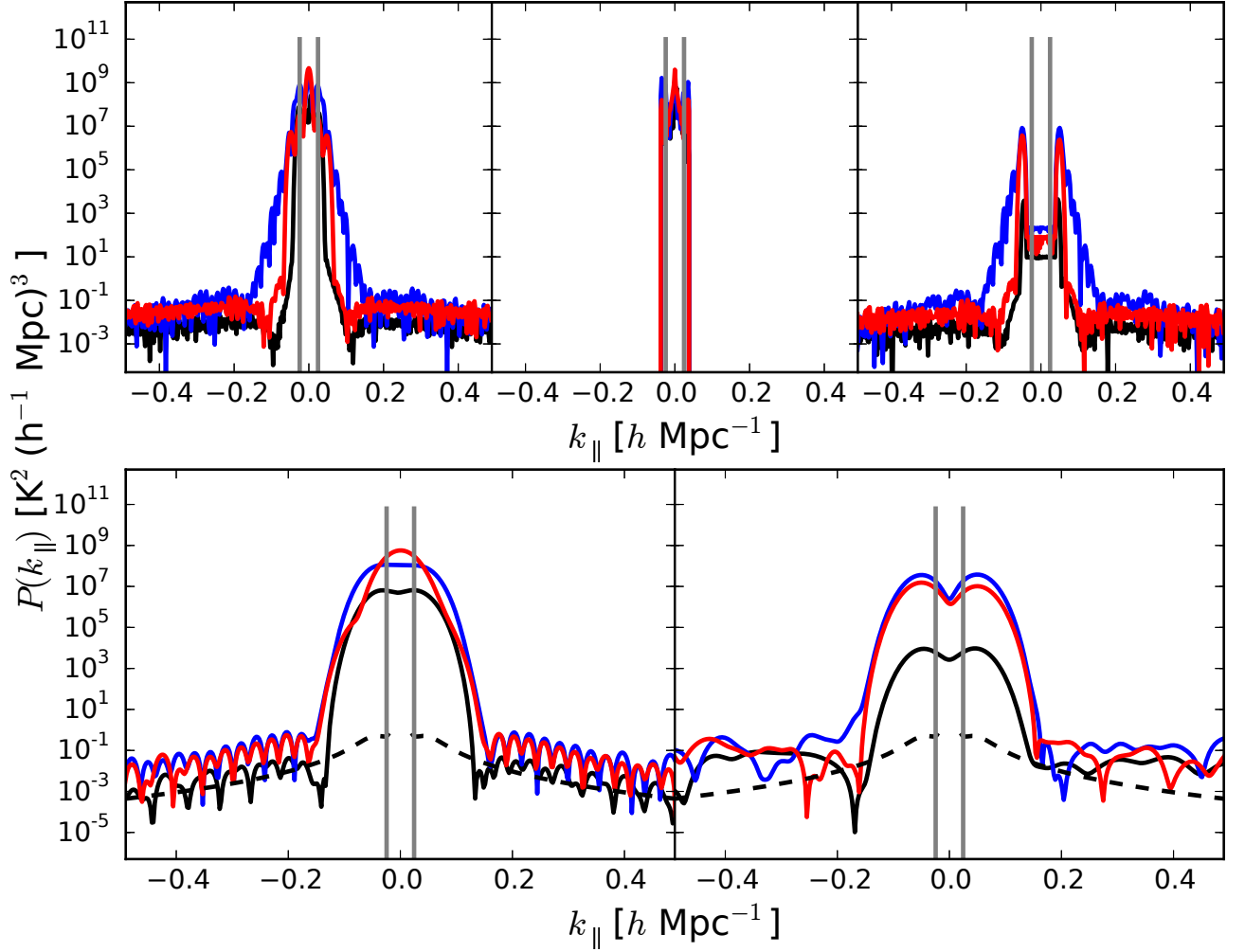
Figure 3. Effect of chromaticity of antenna power pattern on foreground delay power spectra for a 14.6 m baseline.

convolution is narrower than the extent of spillover along $k_\parallel$. The two peaks on either side is most severe for the simulated disk pattern followed by that for the *Airy* disk pattern and least for an achromatic power pattern.

We investigate the effect of chromaticity of power pattern in a foreground avoidance strategy that avoids the aforementioned deconvolution of delay spectrum. Application of window functions with high sidelobe suppression have been discussed for mitigating foreground contamination (Thyagarajan et al. 2013). In line with the foreground avoidance strategy, the visibilities from the full band foreground simulation (whose delay power spectrum is shown on the top left) are multiplied by a Blackman-Harris window function of 10 MHz effective bandwidth. The delay power spectra so produced are shown in the panel on the bottom left. Due to the decreased effective bandwidth the resolution of the delay power spectrum appears decreased. Hence, only the $|k_\parallel| \gtrsim 0.14\, h\, \mathrm{Mpc}^{-1}$ modes remain accessible. Due to the overall lower amplitude of the *Airy* power pattern relative to the simulated dish power pattern and the achromatic pattern, the sidelobe levels of foreground delay power spectra from an *Airy* pattern are lower than the other models by almost two orders of magnitude.

Following a delay-deconvolution based foreground re-

moval strategy, we apply the Blackman-Harris window of effective bandwidth 10 MHz on the unsubtracted foreground residuals (top right panel) in frequency domain and obtain the delay power spectrum shown in the bottom right panel. It is noted that lesser the chromaticity the more effective the deconvolution process is in lowering the residuals in and around the horizon limits. For instance, the peak of the delay power spectrum using the achromatic beam is lowered by four orders of magnitude relative to the original peak whereas the residuals of delay power spectra with chromatic *Airy* and simulated power patterns is lowered only by two orders of magnitude. However, owing to the ineffective subtraction of the response extended beyond the horizon limits, the sidelobe levels have not been lowered significantly and are within an order of magnitude of each other.

In both strategies, the EoR Hɪ signal power spectrum obtained by simulations with 21cmFAST (Mesinger et al. 2008) is shown for reference (dashed black lines) in the bottom panels.

5.3. *Constraints on Reflections between Antennas*

Patra et al. 2015 (submitted) and Ewall-Wice et al. 2015 (submitted) discuss the measured and simulated reflections between a dish and its feed.
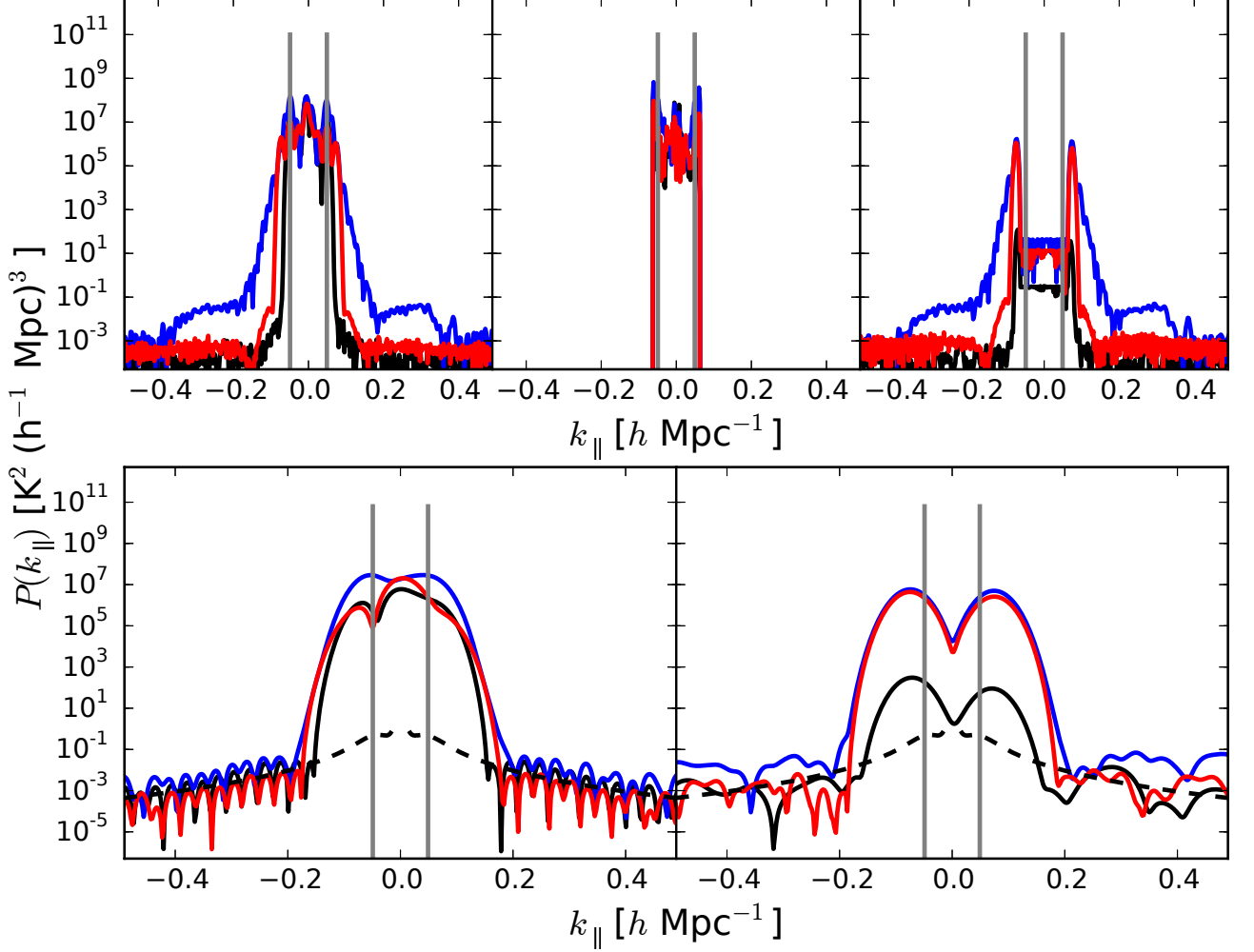
Figure 4. Effect of chromaticity of antenna power pattern on foreground delay power spectra for a 29.2 m baseline.

We provide a related discussion by estimating the attenuation in power required to keep the foreground power reflected between adjacent antennas below the expected EoR Hɪ signal level for the different models of power patterns used in our study.

The effect of reflections it to shift the measured foreground power to higher modes in τ (or equivalently in $k_\parallel$) and thus cause further contamination in these higher $k_\parallel$ modes which are considered sensitive for EoR Hɪ signal detection. Here we estimate the attenuation required at specific $k_\parallel$ modes of interest to contain reflected foreground power between antennas below expected EoR Hɪ power, both corresponding to a 14.6 m antenna spacing.

We define the required attenuation as the ratio:

$$\Gamma_{k_\parallel}(\tau) = \frac{P_{\mathrm{HI}}(k_\parallel)}{P_{\mathrm{FG}}(k_\parallel - \frac{\mathrm{d}k_\parallel}{\mathrm{d}\tau}\,\tau)}, \qquad (3)$$

where, $P_{\mathrm{HI}}(k_\parallel)$ is the EoR Hɪ power spectrum for the chosen antenna spacing, $P_{\mathrm{FG}}(k_\parallel)$ is the foreground delay power spectrum obtained with a Blackman-Harris window function applied over the full band of the three uniquely oriented 14.6 m antenna spacings further averaged over a 0–12 hr LST range and over both positive and negative $k_\parallel$ modes, τ is the delay caused by reflec-

tions, and $\mathrm{d}k_\parallel/\mathrm{d}\tau$ is the *jacobian* in the transformation of τ to $k_\parallel$.

Fig. 5 shows $\Gamma_{k_\parallel}(\tau)$ (in dB) for selected $k_\parallel$ at $0.08\ h\ \mathrm{Mpc}^{-1}$ (left), $0.1\ h\ \mathrm{Mpc}^{-1}$ (middle), and $0.12\ h\ \mathrm{Mpc}^{-1}$ (right) as a function of delays due to reflections from other antenna spacings. The light, medium and dark shaded curves show $\Gamma_{k_\parallel}(\tau)$ for achromatic, *Airy*, and chromatic antenna power patterns respectively. These curves set an upper limit to the reflected foreground power below the EoR Hɪ signal power as a function of delays caused by antenna-to-antenna reflections. It is noted that a chromatic simulated power pattern sets the most severe upper limit in all three chosen $k_\parallel$ for delays $\tau < 80$ ns (left), $\tau < 120$ ns (middle), and $\tau < 160$ ns.

The required attenuation is also a sensitive function of the chosen $k_\parallel$ mode. For instance, at $k_\parallel = 0.08\,h\,\mathrm{Mpc}^{-1}$, the reflections with delays 70 ns require to be attenuated by at $\gtrsim 85$ dB for the simulated power pattern, $\gtrsim 82$ dB for the *Airy* pattern, and $\gtrsim 70$ dB for the achromatic pattern. However, at $k_\parallel = 0.1\,h\,\mathrm{Mpc}^{-1}$ for the same delay of reflection, the requirement on attenuation is lowered to $\gtrsim 75$ dB, $\gtrsim 30$ dB and $\gtrsim 22$ dB respectively. If the chosen $k_\parallel$ is instead $0.12\,h\,\mathrm{Mpc}^{-1}$, the required attenua-
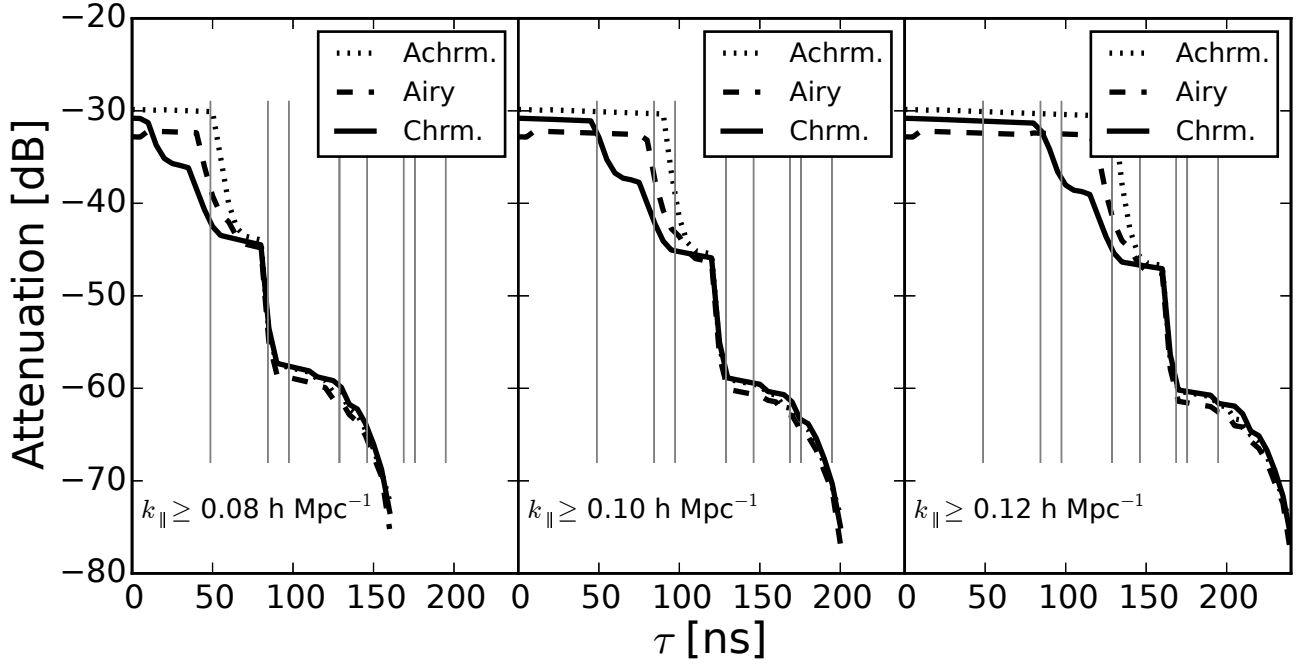
Figure 5. Attenuation of foreground power (in dB) from antenna-to-antenna reflections required to keep the reflected foreground power below EoR Hɪ signal power.

tion is further relaxed to $\gtrsim 60$ dB, $\gtrsim 15$ dB and $\gtrsim 15$ dB respectively. This further reinforces the significance of reducing the chromaticity of the antenna power pattern to further relax the constraint on the system to achieve the attenuation required to contain the reflected foreground power from other antennas from contaminating the sensitive EoR Hɪ signal modes in the *EoR window*.

6. SUMMARY

REFERENCES

Ali, S. S., Bharadwaj, S., & Chengalur, J. N. 2008, MNRAS, 385, 2166
Beardsley, A. P., Hazelton, B. J., Morales, M. F., et al. 2013, MNRAS, 429, L5
Bernardi, G., de Bruyn, A. G., Brentjens, M. A., et al. 2009, A&A, 500, 965
Bernardi, G., de Bruyn, A. G., Harker, G., et al. 2010, A&A, 522, A67
Bock, D. C.-J., Large, M. I., & Sadler, E. M. 1999, AJ, 117, 1578
Bowman, J. D., Morales, M. F., & Hewitt, J. N. 2009, ApJ, 695, 183
Bowman, J. D., Cairns, I., Kaplan, D. L., et al. 2013, PASA, 30, 31
Condon, J. J., Cotton, W. D., Greisen, E. W., et al. 1998, AJ, 115, 1693
Datta, A., Bowman, J. D., & Carilli, C. L. 2010, ApJ, 724, 526
de Oliveira-Costa, A., Tegmark, M., Gaensler, B. M., et al. 2008, MNRAS, 388, 247
Di Matteo, T., Perna, R., Abel, T., & Rees, M. J. 2002, ApJ, 564, 576
Dillon, J. S., Liu, A., & Tegmark, M. 2013, Phys. Rev. D, 87, 043005
Dillon, J. S., Liu, A., Williams, C. L., et al. 2014, Phys. Rev. D, 89, 023002
Furlanetto, S. R., & Briggs, F. H. 2004, New A Rev., 48, 1039
Furlanetto, S. R., Oh, S. P., & Briggs, F. H. 2006, Phys. Rep., 433, 181
Ghosh, A., Prasad, J., Bharadwaj, S., Ali, S. S., & Chengalur, J. N. 2012, MNRAS, 426, 3295
Gleser, L., Nusser, A., & Benson, A. J. 2008, MNRAS, 391, 383
Iliev, I. T., Shapiro, P. R., Ferrara, A., & Martel, H. 2002, ApJ, 572, L123
Liu, A., Parsons, A. R., & Trott, C. M. 2014a, Phys. Rev. D, 90, 023018
—. 2014b, Phys. Rev. D, 90, 023019
Liu, A., & Tegmark, M. 2011, Phys. Rev. D, 83, 103006
Liu, A., Tegmark, M., Bowman, J., Hewitt, J., & Zaldarriaga, M. 2009, MNRAS, 398, 401
Lonsdale, C. J., Cappallo, R. J., Morales, M. F., et al. 2009, IEEE Proceedings, 97, 1497
Madau, P., Meiksin, A., & Rees, M. J. 1997, ApJ, 475, 429
Mauch, T., Murphy, T., Buttery, H. J., et al. 2003, MNRAS, 342, 1117
McQuinn, M., Zahn, O., Zaldarriaga, M., Hernquist, L., & Furlanetto, S. R. 2006, ApJ, 653, 815
Morales, M. F., Bowman, J. D., & Hewitt, J. N. 2006, ApJ, 648, 767
Morales, M. F., Hazelton, B., Sullivan, I., & Beardsley, A. 2012, ApJ, 752, 137
Morales, M. F., & Hewitt, J. 2004, ApJ, 615, 7
Neben, A. R., Bradley, R. F., Hewitt, J. N., et al. 2015, ArXiv e-prints, arXiv:1505.07114
Paciga, G., Albert, J. G., Bandura, K., et al. 2013, MNRAS, 433, 639
Parsons, A. R., & Backer, D. C. 2009, AJ, 138, 219
Parsons, A. R., Pober, J. C., Aguirre, J. E., et al. 2012, ApJ, 756, 165
Parsons, A. R., Backer, D. C., Foster, G. S., et al. 2010, AJ, 139, 1468
Pober, J. C., Parsons, A. R., Aguirre, J. E., et al. 2013, ApJ, 768, L36
Santos, M. G., Cooray, A., & Knox, L. 2005, ApJ, 625, 575
Scott, D., & Rees, M. J. 1990, MNRAS, 247, 510
Sunyaev, R. A., & Zeldovich, Y. B. 1972, A&A, 20, 189

Taylor, G. B., Carilli, C. L., & Perley, R. A., eds. 1999,
    Astronomical Society of the Pacific Conference Series, Vol. 180,
    Synthesis Imaging in Radio Astronomy II
Thyagarajan, N., Udaya Shankar, N., Subrahmanyan, R., et al.
    2013, ApJ, 776, 6
Thyagarajan, N., Jacobs, D. C., Bowman, J. D., et al. 2015a,
    ApJ, 807, L28
—. 2015b, ApJ, 804, 14
Tingay, S. J., Goeke, R., Bowman, J. D., et al. 2013, PASA, 30, 7

Tozzi, P., Madau, P., Meiksin, A., & Rees, M. J. 2000, ApJ, 528,
    597
Trott, C. M., Wayth, R. B., & Tingay, S. J. 2012, ApJ, 757, 101
van Haarlem, M. P., Wise, M. W., Gunst, A. W., et al. 2013,
    A&A, 556, A2
Vedantham, H., Udaya Shankar, N., & Subrahmanyan, R. 2012,
    ApJ, 745, 176
Wang, X., Tegmark, M., Santos, M. G., & Knox, L. 2006, ApJ,
    650, 529
Zaldarriaga, M., Furlanetto, S. R., & Hernquist, L. 2004, ApJ,
    608, 622